Upgrading the Field-Imaging Far-Infrared Line Spectrometer for the Stratospheric Observatory for Infrared Astronomy with kinetic inductance detectors: enabling large sample (extragalactic) surveys

Sebastian Colditz,[a,*] Leslie W. Looney,[b] Frank Bigiel,[c] Christian Fischer,[a] Jacqueline Fischer,[d] Steven Hailey-Dunsheath,[e] Rodrigo Herrera-Camus,[f] Alfred Krabbe,[a] Henry LeDuc,[g] Tony Wong,[b] and Jonas Zmuidzinas[e]

[a]Universität Stuttgart, Deutsches SOFIA Institut, Stuttgart, Germany
[b]University of Illinois, Department of Astronomy, Urbana, Illinois, United States
[c]Universität Bonn, Argelander-Institut für Astronomie, Bonn, Germany
[d]George Mason University, Department of Physics and Astronomy, Fairfax, Virginia, United States
[e]California Institute of Technology, Pasadena, California, United States
[f]Universidad de Concepción, Barrio Universitario, Departamento de Astronomía, Concepción, Chile
[g]Jet Propulsion Laboratory, California Institute of Technology, Pasadena, California, United States

Abstract. We present the initial design, performance improvements, and science opportunities for an upgrade to the Field-Imaging Far-Infrared Line Spectrometer (FIFI-LS). FIFI-LS efficiently measures fine structure cooling lines, delivering critical constraints of the interstellar medium and star-forming environments. The Stratospheric Observatory for Infrared Astronomy (SOFIA) provides the only far-infrared (FIR) observational capability in the world, making FIFI-LS a workhorse for FIR lines, combining optimal spectral resolution and a wide velocity range. Its continuous coverage of 51 to 203 μm makes FIFI-LS a versatile tool to investigate a multitude of diagnostic lines within our galaxy and in extragalactic environments. The sensitivity and field of view (FOV) of FIFI-LS are limited by its 90s-era photoconductor arrays. These limits can be overcome by upgrading the instrument using the latest developments in kinetic inductance detectors (KIDs). KIDs provide sensitivity gains in excess of 1.4 and allow larger arrays, enabling an increase in pixel count by an order of magnitude. This increase allows a wider FOV and instantaneous velocity coverage. The upgrade provides gains in point source observation speed by a factor >2 and in mapping speed by a factor >3.5, enabled by the improved sensitivity and pixel count. This upgrade has been proposed to NASA in response to the 2018 SOFIA Next Generation Instrumentation call. [DOI: 10.1117/1.JATIS.7.2.025002]

Keywords: integral field spectroscopy; kinetic inductance detectors; far-infrared; FIFI-LS; SOFIA.

Paper 20162AS received Nov. 3, 2020; accepted for publication Apr. 1, 2021; published online Apr. 22, 2021.

1 Introduction

The Field-Imaging Far-Infrared Line Spectrometer (FIFI-LS)[1] is the sensitive medium resolution ($R \sim 1500$) spectrometer for the Stratospheric Observatory for Infrared Astronomy (SOFIA).[2] FIFI-LS operates two spectral channels from 51 to 125 μm and 115 to 203 μm simultaneously. It allows fast mapping of the fine structure cooling lines of the interstellar medium (ISM) and

*Address all correspondence to Sebastian Colditz, colditz@dsi.uni-stuttgart.de

in star forming environments within and outside of our galaxy. Its wide instantaneous velocity coverage also allows sensitive observations of more distant galaxies that are just resolved by SOFIA's 2.5 m class telescope. The airborne observatory SOFIA provides routine access to its instrument suite, allowing for servicing, exchange, and upgrade of the instruments. This is a major advantage in comparison to space observatories, which usually cannot be upgraded.

The upgrade of FIFI-LS to FIFI+LS presented in this paper is designed to make the best use of this advantage to improve the observatories scientific capabilities and efficiency. Based on the development of new kinetic inductance detector (KID) arrays, the upgrade will enable point source sensitivity gains of a factor of at least 1.4 (potentially up to 2.5) and gains in mapping speed by a factor of at least 3.5 (potentially up to 12). These gains will enable SOFIA observations that would otherwise be infeasible due to the amount of observing time necessary. We have proposed the upgrade presented in this paper, including a Legacy Science Program to NASA, in response to the SOFIA Next Generation Instrumentation call 2018. The response of the review board relayed to us was generally favorable; however to date NASA has not made a decision. In Sec. 2, we give an overview of the solid basis of our upgrade concept: the FIFI-LS instrument as it is currently operated on SOFIA. We present the anticipated performance improvements and the details of the upgrade concept in Sec. 3. In Sec. 4, we show how the upgrade would open new scientific opportunities.

2 FIFI-LS: The Solid Basis

2.1 *FIFI-LS Overview*

In-depth information on FIFI-LS was published by Fischer et al.[1] and Looney et al.[3] Here we give a coarse overview of the instrument design, concentrating on subsystems and concepts that are relevant to the instrument upgrade.

FIFI-LS is a dual-channel imaging spectrometer. Both spectral channels operate simultaneously, allowing observations of two spectral lines at the same time. The long-wavelength (red) channel operates between 115 and 203 μm and the short-wavelength (blue) channel between 51 and 125 μm. The instantaneous spectral coverage is 750 to 2350 km/s (0.51 to 0.90 μm) in the red and 800 to 3000 km/s (0.19 to 0.71 μm) in the blue channel, depending on the observed wavelength. The complete spectral range of the instrument could be covered with about 125 settings in the red and 170 settings in the blue channel, without overlap. The spectral resolution is also wavelength dependent and ranges from 150 to 550 km/s (0.04 to 0.16 μm). Spatially, each channel has a 5×5 spatial pixel (spaxel) field of view (FOV). In the red channel, the spaxel size on the sky corresponds to 12.2×12.5 square arc sec, in the blue channel to 6.14×6.25 square arc sec.

Both channels are equipped with a reflective integral field unit (IFU), which reorganizes the square 5×5 spaxel FOV into a $(25 + 4) \times 1$ spaxel slit, which is coupled into a quasi-Littrow mounted spectrometer. Figure 1 shows the IFU and a schematic of how the two-dimensional FOV is reorganized into a one-dimensional slit. The IFU comprises three sets of five mirrors each. The first set is the slicer mirrors. These mirrors are in a focal plane of the instrument. They slice the 5×5 spaxel FOV into five image slices and reimage the entrance pupil for each slice onto one of the five capture mirrors, which form the second set of mirrors. The capture mirrors are positioned in the plane of a pupil image. Each of the five mirrors refocuses its slice onto a slit mirror in the third set of mirrors of the IFU. Therefore, the slit mirrors are again in a focal plane. The focused image of the slit has a length of $25 + 4$ spaxels at this position. The space for the four additional spaxels is gaps between the five individual slices. These gaps are introduced to avoid crosstalk between the edges of the slices. Finally, the slit mirrors ensure that the pupil image of each slice is correctly centered on the grating once it passes the collimating optics. The dispersing element in each spectrometer channel is a reflective grating. Each grating may be rotated within a total range of about 40 deg at sub-arc second precision, to select the observed wavelength. The gratings have been optimized for their specific wavelength ranges. The simulated grating efficiencies are shown in Fig. 2. Especially, the blue channel grating is highly polarizing toward the ends of the covered wavelengths. The polarization has to be taken

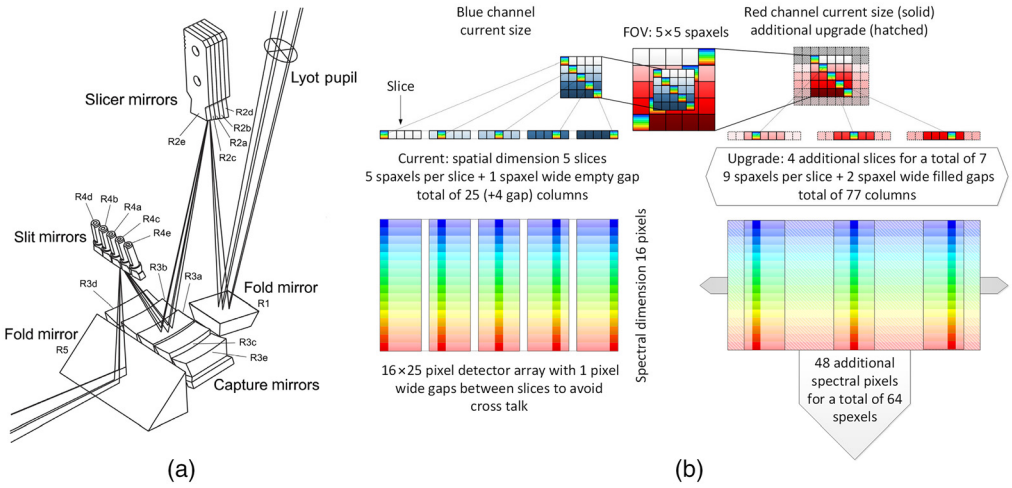

Fig. 1 IFU concept of FIFI-LS. (a) Close-up view of the IFU mirror components for the red channel with the rays for the central slice shown.[3] The blue channel is similar. (b) Illustration of the field-imaging concept in FIFI-LS. The 5×5 spaxel FOV imaged in the plane of the slicer mirrors is sliced into five slices and reorganized on a $(25 + 4) \times 1$-spaxel pseudoslit, imaged in the plane of the slit mirrors. The pseudoslit is dispersed along the spectral direction in the spectrometer optics and imaged onto the 400-pixel detector with 25 pixels in the spatial direction along the slit and 16 pixels in spectral direction perpendicular to the slit. The rainbow colored spaxels and highlighted columns of spectral pixels (spexels) give an idea on how the spatial information of the spaxels is reorganized and finally spectrally dispersed. The right side of the schematic shows how the FOV and detector size could be increased for FIFI+LS; this is explained in Sec. 3.

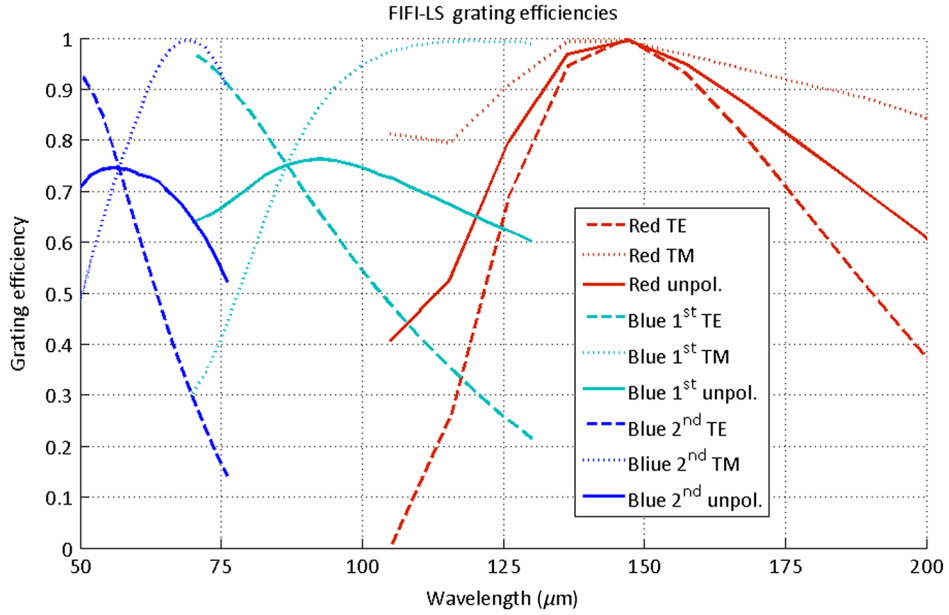

Fig. 2 Simulated grating efficiencies of the FIFI-LS gratings. The red channel operates in first order only, for the blue channel first and second orders are used—in operation, a filter changer switches between filter sets optimized for either order. The gratings have polarizing effects. The TE polarization has the *E*-field parallel to the grating grooves, whereas the TM polarization has the *E*-field perpendicular to the groves. Simulation by Norbert Geis, Max Planck Institute for Extraterrestrial Physics.

into account when optimizing the new detector arrays, when pixels have polarization dependent quantum efficiency (QE).

The core of the instrument is its two 400-pixel gallium-doped germanium photoconductor detector arrays.[4] Each array is assembled from 25 modules—one for each spaxel—with 16 pixels

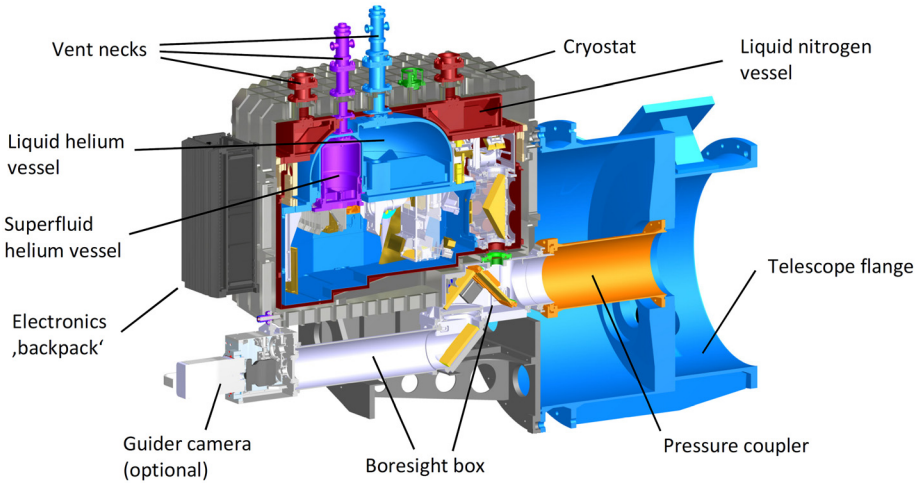

Fig. 3 CAD drawing of the FIFI-LS cryostat attached to the SOFIA telescope flange.[1]

in the spectral direction. For the red channel, the modules have been specially designed to apply strong uniform stress to the 16 pixels in order to shift their spectral response toward longer wavelengths. The modules in the blue channel apply only enough stress to ensure the mechanical stability of the pixel stack. The detectors have been assembled pixel by pixel, manually. The pixel yield is >95%. The photon dominated NEP of the detectors is about 5×10^{-17} W Hz$^{-1/2}$. The dark NEP is about 5×10^{-18} W Hz$^{-1/2}$.[4] The QE as inferred from measurements assuming background limited performance ranges from 25% to 35%.[3] Light is coupled to the individual pixels via funnel shaped light cones. The area of a pixel in the focal plane of the detector is about 3.9×3.9 mm^2. Each detector module is read out by a cold read-out electronic (CRE) circuit. The CREs are specially designed complementary metal–oxide–semiconductor (CMOS) circuits, originally developed for the Herschel-photodetector array camera & spectrometer (PACS).[5] The detector current is read out by a capacitive feedback, integrating amplifier. A sample-and-hold circuit within the CRE acts as analog memory between integrator and multiplexing circuit. The capacitor voltages are sampled with a rate of 250 Hz. The measurement is done in a sampling up the ramp technique, typically resetting the capacitor voltage every 32 samples. Therefore, the detector electronics supply a rate of about 7.8 ramps per second with 32 samples on each ramp.

Both detectors are cooled to temperatures of 1.6 K to attain the NEP mentioned above. The spectrometer optics are cooled to 6 K and the entrance optics to 77 K, reducing the thermal background within the instrument. Cooling of the instrument is accomplished by the four-layer bath cryostat design shown in Fig. 3. The first layer is the evacuated cryostat shell at room temperature. The second layer is cooled to 70 K by a 25-L liquid nitrogen vessel attached to a radiation shield and the optical bench for the entrance optics. On the third layer, the cooling is provided by a 35-L liquid helium vessel. The optical bench with the IFU and spectrometer optics belongs to this level. Due to the heat influx and the heat produced on the optical bench by electronic components, the temperature is typically 6 K, which is slightly higher than the boiling temperature of liquid helium at 4 K. The innermost layer is occupied by the two 400 pixel detector arrays and the CREs. This layer is cooled by a small 2.8-L superfluid liquid helium vessel. This vessel is pumped in order to attain the operating temperature of 1.6 K.

2.2 *Science with FIFI-LS*

With its sensitivity (see Fig. 4), wavelength coverage, spectral and spatial resolution, FIFI-LS plays a major role in investigations of the ISM both extragalactic and within our galaxy, as well as for investigations of (primarily massive) star formation since 2014. The wide wavelength coverage of FIFI-LS allows the observation of a multitude of diagnostic lines in the far-infrared (FIR). Table 1 lists all lines observed to date. The key features observed most often with FIFI-LS are the bright FIR fine structure lines of [CII] at 158 μm, [OI] at 63 and 146 μm, [OIII] at 52 and 88 μm, [NII] at 122 μm, [NIII] at 57 μm, and molecular lines like the CO rotational lines from

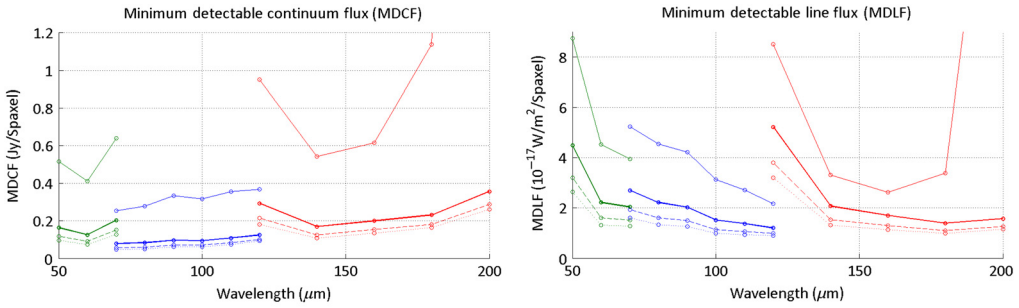

Fig. 4 Sensitivities of FIFI-LS[6] (thin solid lines) and FIFI+LS modeled upgrade sensitivities (thick solid, dashed, and dotted lines). The values are calculated for an S/N of 4 in 900 s on-source integration time, not including the larger FOV of FIFI+LS. A penalty of $\sqrt{2}$ is included in all values to account for the differential observation schemes typical for FIR observations. (a) The minimum detectable continuum flux assuming that all spectral pixels are coadded for a single spatial pixel. (b) The minimum detectable line flux when using the optimal number of spectral pixels to retrieve a line for pure detection. The thick solid lines are the baseline for the FIFI+LS upgrade assuming similar quantum efficiencies for the new KID-arrays and the current detectors. The dashed/dotted lines would result from the KID-arrays realizing double (~60%)/triple (~90%) the QE of the current setup. The spectral coverage in the blue channel is achieved using first or second diffraction order of the reflective gratings (green and blue curves). The spectral coverage in the red channel uses first diffraction order (red curves). Toward 200 μm, the KID-arrays are expected to perform much better than the current detectors, which have a cutoff wavelength close to 200 μm.

Table 1 Spectral lines observed with FIFI-LS[1]—there are no gaps in FIFI-LS's wide spectral coverage, allowing the observation of a multitude of diagnostic lines in the FIR.

Line	λ (μm)	Line	λ (μm)	Line	λ (μm)	Line	λ (μm)	Line	λ (μm)
[OIII]	51.8	CO	70.9	CH4	87.3	CO	124.2	OH	163.3
OH	55.9	CO	77.1	[OIII]	88.4	CO	130.4	HCN	169.4
[NIII]	57.3	CH_4	80.1	OH	96.3	[OI]	145.5	CO	174
[OI]	63.2	CO	84.4	CO	96.8	CO_2 (ice)	146	CO	186
C_2H_2	68.6	OH	84.5	CO	104.4	CO	153.3	CO	200.3
CO	69.1	CO_2 (ice)	86	CO	118.6	[CII]	157.7		
C_2H_2	69.7	CO	87.2	[NII]	122	CO	162.8		

$J = 13$ to 12 up to $J = 38$ to 37. FIFI-LS observations also provide the underlying continuum flux for sufficiently bright objects. Below, we summarize a few of the published FIFI-LS results.

FIFI-LS has efficiently mapped complete galaxies in [CII], to study how star formation rates and [CII] emission correlate in different environmental conditions. For example, Pineda et al.[7] probed the relationship between SFR and [CII] over a wide range of conditions by mapping the whole disk of the M51 galaxy including its companion M51b. The preliminary results are that SFR and [CII] emission are well correlated over the disk of M51 including the center, spiral arms, and interarm regions, in good agreement with the KINGFISH galaxy relationship.[8] However, the M51b galaxy shows a significant deficit of [CII] emission with respect to the SFR rate estimated from FIR-continuum. M51b is a barred lenticular galaxy in a poststarburst phase, in which massive star-formation is suppressed.[9] The lack of massive star formation in M51b is consistent with the faint [CII] emission detected, but it is inconsistent with the large SFR estimated in this galaxy. The bright 24-μm dust continuum emission, which dominates the SFR estimate, is likely heated by an active galactic nucleus, therefore not tracing star formation activity. The observed [CII] deficit in M51b suggests that this galaxy is a nearby analog

of ultra-luminous infrared galaxies and represents an important laboratory, in which to study the origin of the [CII] deficit observed in these galaxies.

Bigiel et al.[10] presented the results for another full-galaxy [CII] map with FIFI-LS of the nearby spiral galaxy NGC6946. The data allowed disentangling the [CII] luminosities of the arms (73%), center (19%), and interarm regions (8%) of NGC6946. A comparison of the radial profiles of [CII] emission to various gas and star formation rate tracers ([CII]/TIR, [CII]/CO, and [CII]/PAH) reveals a pronounced "[CII]-deficit" in the center. In combination with models, a radially declining trend of alpha_CO is found, reflecting the radially declining metallicity gradient in this galaxy. Finally, the overall low alpha_CO values argue for a surprisingly low-dark molecular gas content in this galaxy, which is in contrast to estimates in the Milky Way.

FIFI-LS has also studied the [CII] emission in relation to other SFR tracers in multiple other galaxies. One example are the observations of the central region of the active galaxy NGC 4258 by Appleton et al.[11] The results suggest that a significant share of the [CII] emission from NGC 4258 is not associated with star formation but is excited by shocks and turbulence induced by the highly inclined jet of the galaxy. Observing with FIFI-LS, Smirnova-Pinchukova et al.[12] found excessive [CII] emission in an active galactic nucleus (AGN) galaxy as a likely signature of an AGN-driven outflow.

Observations of the galactic center presented by Iserlohe et al.[13] showed how the ability of FIFI-LS to quickly map large areas in multiple fine diagnostic lines was used to characterize photodissociation regions (PDR). Line emission maps of four lines: [CII], [OI] 63 and 145 μm, and CO $J = 14$ to 13 as well as the FIR flux derived using FIFI-LS, FORCAST,[14] and PACS continuum data were used to infer the density and FUV-field using PDR models.[15] The analysis by Iserlohe et al. shows that the [OI] line fluxes at ~63 μm have to be affected by self-absorption, whereas there is significant contribution to the [CII] line flux not originating from the probed PDR. The ability to measure the [OI] line at 145 μm and the CO line in addition to [CII] and [OI] at 63 μm were the key to derive the correct PDR parameters.

3 FIFI+LS: The Next Level

3.1 *Concept Overview and Estimated Performance Improvements*

The sensitivity, FOV, and instantaneous spectral coverage of FIFI-LS are currently limited by its 90s-era photoconductor arrays. All of these performance parameters can be improved significantly by upgrading the instrument with new KID arrays. These arrays may be produced with an order of magnitude more pixels, enabling the increase of the FOV and the instantaneous spectral coverage of the instrument. KIDs have less generation–recombination ($g - r$) noise than photoconductors, which translates into a $\sqrt{2}$ sensitivity gain for background-limited operation. Sensitivity data for the current FIFI-LS instrument[6] and the modeled sensitivities of the upgrade are shown in Fig. 4. The baseline improvement model (thick solid line) relies on the negligible $g - r$-noise; further improvements are possible by increasing the QE of the KIDs beyond the ~30% of the current FIFI-LS detectors.

The presented instrument upgrade concept, called FIFI+LS, will maximize the science output while keeping cost and development time low by utilizing most of the original FIFI-LS design and components. This is possible because the original instrument design anticipated future detector upgrades and the entrance optics were designed to accommodate a larger FOV. Table 2 shows the baseline parameters for the FIFI+LS upgrade in comparison to the current FIFI-LS instrument.

On the detector level, the instrument's sensitivity will improve by a factor of 1.4 to 2.5. The lower end of the estimate is the gain from the reduced $g - r$-noise. Additional gains are expected from improvements of the QE. The current FIFI-LS detectors have a QE of 25% to 35%.[4] Depending on the implementation, the new KIDs arrays could yield QEs of 40% to 80%. The FOV of the instrument will increase by a factor of 1.75. This increase will enable faster mapping and more efficient observation modes (e.g., Lissajous scanning).

The increased number of spectral pixels will have three distinct advantages. (1) It will facilitate the observation of wide lines, especially in extragalactic sources, providing overall better

Table 2 Upgraded FIFI+LS instrument parameters compared to FIFI-LS.

	FIFI+LS blue chan.	FIFI+LS red chan.	FIFI-LS blue chan.	FIFI-LS red chan.
Wavelength range (μm)	51 to 125	115 to 206	51 to 125	115 to 203
Spect. res. (km/s)	130 to 435	155 to 425	155 to 550	160 to 425
Spect. res. (μm)	0.03 to 0.10	0.11 to 0.16	0.04 to 0.13	0.11 to 0.16
Instant spect. range (km/s)	2500 to 9000	3200 to 10,000	800 to 3000	750 to 2350
Instant spect. range (μm)	0.59 to 2.13	2.20 to 3.84	0.19 to 0.71	0.51 to 0.90
Settings to cover full range[a]	~60	~35	~170	~125
FOV (arc sec)	45×35	90×70	30×30	60×60
Spatial pixels	9×7	9×7	5×5	5×5
Spatial pixel pitch (arc sec)	5	10	6	12
Spect. pixels per spaxel	64	64	16	16
Image slices	7	7	5	5
Detector width (pixel)[b]	$(9+2) \times 7 = 77$	$(9+2) \times 7 = 77$	$5 \times 5 = 25$	$5 \times 5 = 25$
Detector size (pixel^2)	$77 \times 64 = 4928$	$77 \times 64 = 4928$	$25 \times 16 = 400$	$25 \times 16 = 400$

[a]Theoretical values when scanning the whole respective range without overlap.
[b]Two additional pixels per slice to allow for gaps and avoid crosstalk between slices.

baseline coverage. (2) It will enable the observation of atmospheric water features concurrent with the observations for most of the important FIR-diagnostic lines. This will improve the accuracy of the atmospheric calibration and strongly reduce the overhead necessary for atmospheric calibration observations. (3) The detector may be split into two (or more) sections in spectral direction, each optimized for a subband of the spectral coverage in the respective channel. This will allow increasing the sensitivity at key lines (e.g., [CII] and [OI]). Figure 5 shows the increased spectral coverage close to the [CII] line along with ATRAN[16] models of the atmospheric transmission. The two visible water absorption features are routinely used to measure precipitable water vapor with FIFI-LS[17] at specific times in a flight. FIFI+LS could continually monitor water vapor for [CII] observations in parallel with the astronomical observation with no need for additional observing time.

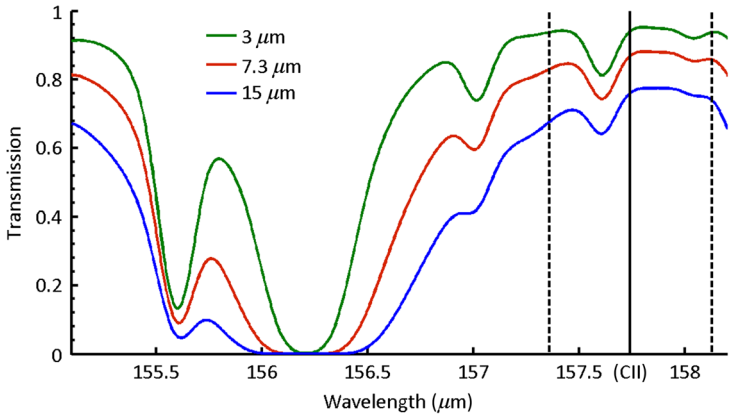

Fig. 5 Atmospheric transmission for three different values of precipitable zenith water vapor close to the [CII] fine structure line. The current instantaneous spectral coverage is within the dashed lines, and the upgrade covers the full spectral width shown. The telluric water features at 155.6 and 156.2 are used for atmospheric calibration.

Through a careful redesign of the spectrometer optics, it will be possible to improve the spectral resolution in the blue channel and to increase the spectral range of the red channel to include the [NII] 205-μm line. In all, we expect the improvements to increase the observing speed by a factor of 3.5 to 12 for compact sources and for mapping. This gain in efficiency will increase the observable universe for SOFIA/FIFI-LS and provide more efficient use of SOFIA's precious observing time.

The three major areas of the instrument that are affected by the upgrade are the detectors and detector readout, the IFU and spectrometer optics, and the cooling concept. The necessary changes are addressed in the following sections.

3.2 *KIDs Arrays*

There have been important improvements in detector technology since FIFI-LS and PACS fielded the largest gallium-doped germanium photoconductor detector arrays (400 pixels), especially in respect to KIDs. The Caltech/JPL group is developing sensitive feedhorn-coupled aluminum KIDs for use at 240 to 420 μm in the balloon borne spectrometer TIM.[18] TIM will deploy ~3600 KIDs using ~1000 pixel subarrays and has an NEP requirement of 1×10^{-17} W Hz$^{-1/2}$, similar to the photon-limited NEP needed for FIFI+LS. TIM prototype detectors have demonstrated NEPs of 4×10^{-18} W Hz$^{-1/2}$,[19] and simulations indicate an 80% dual-polarization optical efficiency across the 317- to 420-μm band.[20] This design will be scaled to the shorter wavelengths of the FIFI+LS red channel. As the responsivity of these KIDs scales inversely with the inductor volume,[19] shrinking the absorber to scale the design to shorter wavelengths will result in a moderate reduction in the NEP. With a factor of 2 reduction in the linear scale and assuming an 80% QE, the detector NEP referenced to the front of the feedhorn for the red channel detectors will be 1.9×10^{-18} W Hz$^{-1/2}$.

The KIDs developed for TIM will also form the basis for the FIFI+LS blue channel detectors but will use a modified absorber and optical coupling scheme appropriate for the shorter wavelengths. Recent simulation work and initial testing was presented by Perido et al.[21] in a study for detectors for the galaxy evolution probe (GEP).[22] Their work addresses KIDs designed for wavelengths between 10 and 100 μm. GEP will need sensitivities as low as 1×10^{-19} W Hz$^{-1/2}$ in this wavelength range, which is much better than what is necessary for FIFI+LS. As with the TIM detectors, Perido et al. were pursuing lumped element aluminum. Their simulation work has shown that thin aluminum film may be patterned on a silicon substrate to produce good optical absorption at wavelengths as short as 10 μm. The short meander design studied by Perido et al.[21] used a 200-nm wide absorber line that is interrupted with a meander to increase the resistance per unit length while simultaneously introducing a distributed capacitance to compensate for the accompanying distributed inductance. For backside illumination, this design achieves a dual-polarization efficiency of 58% over the 10- to 30-μm band, a fractional bandwidth larger than that of the 51- to 125-μm FIFI+LS blue channel spectral range. This absorber geometry will be the starting point of a future optimization targeting the FIFI+LS blue band. The absorber will be illuminated with a microlens equipped with a broadband antireflective layer.

Perido et al.[21] presented dark-noise measurements of KIDs patterned using their short meander design. The noise is dominated by the two-level system (TLS) noise common to KIDs, and when operating at 200 mK the electrical noise is $S_{xx} = 6 \times 10^{-17}$ Hz^{-1}. The detector responsivity was not measured, but following the approach described by Hailey-Dunsheath et al.,[23] conservative assumptions about the aluminum film quality lead to an estimated responsivity of $R_x = 1.8 \times 10^9$ W^{-1} and a TLS-limited NEP of 4.3×10^{-18} W Hz$^{-1/2}$. To operate at the somewhat longer wavelengths of the FIFI+LS blue band, the absorber studied by Perido et al. will be increased to 120 μm in diameter, which represents a factor of 4 increase in the absorber area and a corresponding increase to the NEP. The TLS noise will be reduced, however, by increasing the size of the capacitor. The small size of the capacitor employed by Perido was determined by their 0.4 mm detector pitch, which is significantly smaller than the ~0.8-mm pitch of the FIFI+LS focal plane. A detailed capacitor geometry will be the subject of a future optimization, but it is well established that TLS noise is reduced by increasing the capacitor size,[24] and we expect a factor of 2 reduction in the TLS noise will be readily achieved.

Assuming a 50% QE, this leads to an NEP referenced to the front of the microlens of 1.6×10^{-17} W Hz$^{-1/2}$.

The performance of the FIFI+LS KIDs will be similar to those developed for TIM. The diffraction-limited spot size produced by the microlens on the blue channel detectors will be smaller than the wavelength. Assuming a 125-μm diameter absorber the inductor volume would be a factor of ~3 larger than in the TIM prototypes. The capacitor area would be reduced to maintain the LC resonance frequency at ~300 MHz, and the expected detector NEP would be $\sim 1.5 \times 10^{-17}$ W Hz$^{-1/2}$. The absorber geometry, pixel size, and layout of the microlens and feedhorn arrays for the blue and red channels has to be refined during a further study. In addition, the detector response within the FIFI+LS spectral bands (especially the large bandwidth of the blue channel) has to be optimized and strategies for maximizing array efficiency at the most used wavelengths have to be investigated, all while retaining background-limited performance. One possible strategy is to split the blue channel detector into two sections along the spectral direction. Those sections would be optimized individually (e.g., considering the polarizing effects of the grating shown in Fig. 2).

The switch from background-limited photoconductors to KIDs will improve the point source sensitivity. A photon absorbed in a photoconductor excites a single-charge carrier, and the stochastic recombination of these charge carriers increases the fundamental photon noise by a factor of $\sqrt{2}$. In contrast, a photon absorbed in a KID breaks a large number of superconducting electron pairs (~17 for $\lambda = 100$ μm in an aluminum film), and the associated recombination noise is negligible. Additionally, the absorption efficiency in the FIFI+LS KIDs is anticipated to be ~40% to 80%, an improvement on the 25% to 35% achieved with the FIFI-LS photoconductors. As a result of these two terms, we expect the KID arrays will provide at least a factor of $\sqrt{2}$ sensitivity increase based on the $g - r$ noise reduction and an increase up to a factor of 2.5, if we can realize the 80% QE.

The KIDs arrays will also require a redesign of the readout electronics for the FIFI+LS upgrade. Each KID forms a microwave resonant circuit with changes to the absorbed optical power driving shifts in the resonant frequency. The readout electronics drive each KID at its resonant frequency and determine the frequency shifts by monitoring the complex transmission of the drive tone. We will use the same FPGA-based readout originally developed for the BLAST-TNG instrument[25] and further developed for TIM and other instruments fielding large-format KID arrays.[26]

3.3 *Optics*

The general optical layout of FIFI+LS will remain the same as FIFI-LS. The upgrade will affect the IFU, the collimator optics, and the final detector camera optics. The entrance optics can remain unchanged as they were already designed to support an FOV up to 90 arc sec × 90 arc sec. The diffraction gratings will also be reused for the upgrade. The gratings are already the optimal size for the available space and the groove distance and profile are optimal for the FIFI+LS wavelength range. Not including the detectors, the gratings are the most expensive parts of the instrument optics. Retaining the original gratings saves upgrade costs on the order of $450k.

Each IFU is composed of three sets of mirrors as explained in Sec. 2.1. Each mirror-set contains as many mirrors as there are slices of the FOV. The increase of the FOV from 30 arc sec × 30 arc sec to 45 arc sec × 35 arc sec in the blue channel and from 60 arc sec × 60 arc sec to 90 arc sec × 70 arc sec in the red channel necessitates an increase in spaxel number to sample the FOV sufficiently. The baseline design uses 9×7 spaxels, with 7 slices of 9 spaxels in the IFU. Therefore, the upgraded IFU will need seven instead of five mirrors for each of its three mirror sets. This baseline design of the IFU has already been modeled in the optical software ZEMAX. Figure 6(a) shows this seven-slice model in a view similar to the original setup shown in Fig. 1. The width of the original five-slice IFU setup in Fig. 1 is driven by the capture mirror set, which needs 86 mm. The new seven-slice setup will need 105 mm, driven by the wider fold mirror R5. The capture mirror width for the new setup would be even wider than 105 mm but was reduced by reducing the individual mirror widths. This reduced width still contains the full geometric beam with additional margin for diffraction. The ~20-mm

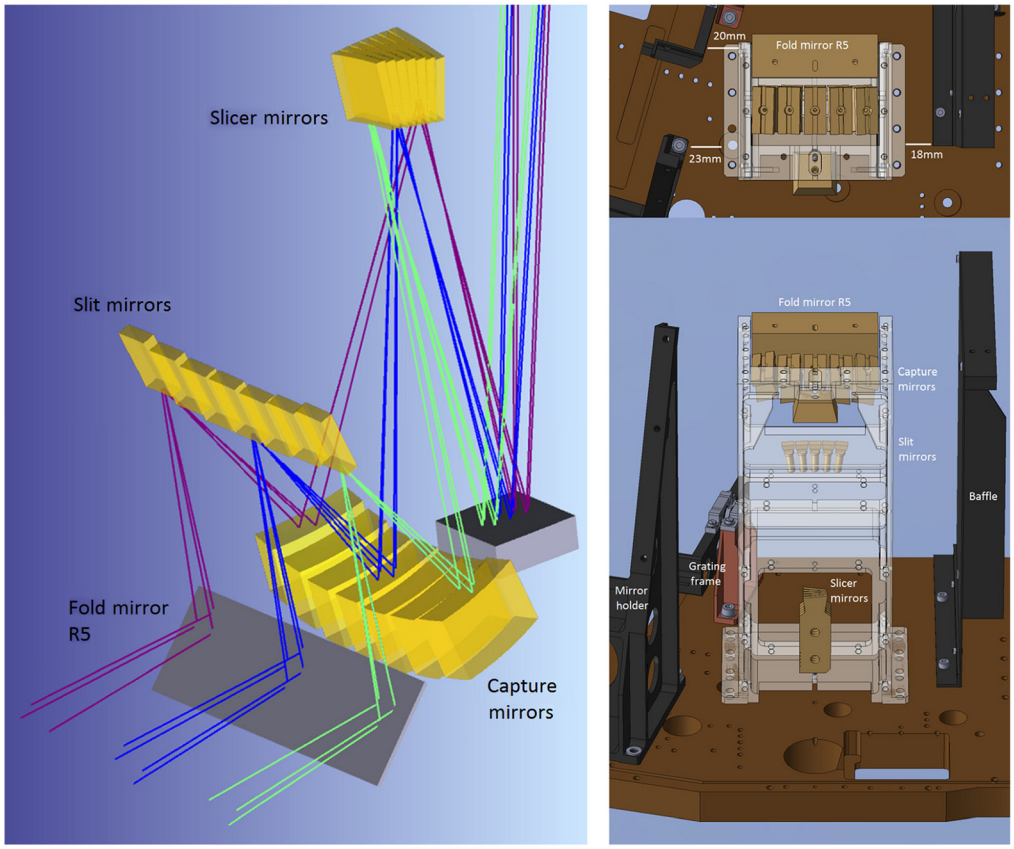

(a) (b)

Fig. 6 (a) Seven-slice IFU concept of FIFI+LS for the red channel. The blue channel is similar. (b) Front-diagonal- (lower image) and top- (upper image) view of the current FIFI-LS five-slice IFU of the red channel. The IFU holder structure is the translucent structure shown. The closest structure to the right of the IFU holder is the center baffle blocking stray light from the blue channel. The closest structures to the left are a mirror holder and the holding frame for the diffraction grating. All structures are more than 10 mm away from the IFU holder.

overall increase in width can be accommodated within the cryostat. The structures closest to the IFU holder are more than 10 mm away on either side. This is visible in the CAD-image in Fig. 6(b). The ZEMAX model shows that the optics will remain diffraction limited even in the corners of the larger FOV. The final optimization of the complete spectrometer optics in both channels has to be done in a future study. The currently baselined spaxel pitch of 5 arc sec in the blue and 10 arc sec in the red channel is a compromise between instantaneous spatial resolution and light losses due to diffraction within the IFU. Within the future study, it has to be determined whether this baseline is the best solution in terms of mapping speed and sensitivity with a full model of the optics.

3.4 *Cooling*

The new KID arrays operate at temperatures below 250 mK, which is considerably lower than the current FIFI-LS detectors' operating temperature of 1.6 K. It will, therefore, be necessary to redesign the instrument cooling. The original cryostat provides four temperature levels: room temperature, liquid nitrogen cooled at 77 K, liquid helium cooled at 6 K, and pumped liquid helium at 1.6 K. The entrance optics are on the 77-K level, the spectrometer optics on the 6-K level, and the detectors on the 1.6-K level.

There are multiple options to realize the necessary detector cooling within the current layout of the FIFI-LS cryostat with different impacts to the overall design. An option with limited impact would only remove the 2.8-L superfluid helium vessel and use the space freed by the

vessel and the KIDS detectors, which are smaller in volume compared to the current photoconductor arrays, to accommodate the new detector cooling systems. A more invasive option would require the removal of the 2.8-L superfluid helium vessel and the 35-L helium vessel. This option uses a pulse tube cryocooler to cool the spectrometer optics and provide the intercept for the detector cooling system. This concept takes advantage of the cryocooler compressors installed on SOFIA, which are used for the cryocooling of upGREAT.[27]

The detector cooling will be realized by an adiabatic demagnetization refrigerator (ADR) to reach temperatures <250 mK. This approach is similar to the approach taken by the SOFIA instrument HAWC+.[28,29] HAWC+ has an estimated detector heat load on the ADR of 5 μW[28] and an additional parasitic load of 18.5 μW[28] excluding vibrational heating. The vibrational heating initially tripled the total heat load on the ADR to ~70 μW.[30] This was greatly reduced by tuning the mechanical resonances of the system. The HAWC+ADR design supplies a 170-mK operating temperature for the duration of complete SOFIA science missions.[29] For our KID arrays, we will aim for higher operating temperatures between 200 and 250 mK. The FIFI+LS baseline detectors have a total of 9856 pixels with an estimated saturation power of 2 pW, which also corresponds to the maximum optical loading expected, resulting in a 20-nW optical load on the detectors. In comparison, the slightly smaller HAWC+ detectors have an estimated background load of 60 pW/pixel giving 230 nW on its three 32×40 pixel detector arrays.[29] HAWC+ routes 822 wires from its 1-K stage to its 170-mK ADR stage for detector readout and housekeeping. The FIFI+LS readout will need a pair of wires for every 750 pixels resulting in only 28 readout wires plus a few additional wires for temperature monitoring. Given these comparative figures between the FIFI+LS baseline design and HAWC+, we are confident that an ADR design similar to the one used in HAWC+ will provide sufficient cooling for the detector stage of FIFI+LS.

The optimal layout for the cryogenic cooling has to be defined in a future study. For the pulse tube option, it needs to be decided whether a standard commercial two-stage option or a custom single-stage option directly coupled to the liquid nitrogen reservoir would be the best. The current heat load on the liquid helium cooled level at 6 K is 1.3 W. TransMIT, the supplier of the upGreat cryocoolers, offers a model that can accommodate 1.17 W at 4.2 K[31] when paired with one of the two compressor systems on SOFIA. We are, therefore, confident that an optimized design will allow accommodating the heat load from the FIFI+LS system at a temperature below the 6-K of the current spectrometer optics. This would reduce the instrument internal background in the red channel. For the detector cooling, the two considered options include a dual-stage ADR system and a He4 or He3 sorption cooler backed single-stage ADR.

4 Science Opportunities

Today, SOFIA provides the only FIR observational capability in the world, which means that FIFI-LS has a prime role as an extragalactic workhorse of FIR spectroscopy (due to its wide spectral coverage). However, FIFI-LS' sensitivity and FOV are limited by its detectors, requiring significant time commitments for large sample observing campaigns, making them often difficult or impossible to achieve in a flight series or two. This has limited the science impact of FIFI-LS on SOFIA. The upgraded FIFI+LS with more sensitive and larger detectors, however, will open a new window into FIR studies of the ISM. With FIFI+LS, it would be possible to create a coherent set of observations of the main FIR fine-structure lines on physical scales that range from a few parsec [e.g., for Small or Large Magellanic Cloud (SMC, LMC) targets] to kiloparsec (for a wide range of galaxies in the nearby universe) scales, over a significant sample that would be complementary to many of the Herschel surveys. Such a program cannot be practically completed today with FIFI-LS, but it would be routinely possible with FIFI+LS.

The FIR fine-structure lines of C, N, and O offer a powerful tool to characterize the ISM of nearby and high-z galaxies.[32–35] These lines arise from both ionized gas and PDRs and include the [CII] 158 μm, [OI] 63 and 145 μm, [NII] 122 and 205 μm, [OIII] 88 and 52 μm, and [NIII] 57 μm transitions. FIFI+LS will provide a unique opportunity to observe all these lines in the Milky Way and nearby galaxies, whereas powerful interferometers such as the Atacama Large Millimeter/Submillimeter Array (ALMA) and the Northern Extended Millimeter Array (NOEMA) will be routinely detecting these lines in galaxies in the $1 < z < 8$ redshift

range.[36,37] Therefore, observations of nearby galaxies with FIFI+LS, where the physical scales probed are much smaller, galaxy samples are larger and ISM properties can be studied in much more detail, are critical as templates to understand and interpret high-z galaxy observations and as an essential link between Milky Way studies and those at high redshift.

Herschel/PACS made important contributions to our understanding of the FIR line emission in nearby galaxies, ranging from dwarf, low-metallicity systems to the densest, heavily obscured and most energetic starburst nuclei and luminous infrared galaxies.[35,38–40] However, PACS has left many key questions unanswered, such as the origin of the FIR line deficit (see below). The only way to address these questions are more comprehensive observations, building on the PACS and FIFI-LS legacy. The superb mapping speed, large FOV, and sensitivity of FIFI+LS opens up entirely new opportunities by making large surveys of nearby and intermediate distance galaxies routinely possible. In combination with multi-wavelength ancillary data, SOFIA/FIFI+LS will create its own legacy by entering a new mode of survey style operations, probing the physical properties of the ISM and the origin of the FIR emission lines in an unprecedented range of parameter space. We have outlined an LSP as part of our NASA Proposal, targeting 43 nearby and intermediate distant galaxies, and 3 star forming regions within the SMC, that cover a wide range of environments and will be a valuable complement to some of Herschel's large surveys (e.g., KINGFISH, SHINING, GOALS, and DGS), covering galaxies not observed with Herschel/PACS in the respective lines and delivering full galaxy disk maps where PACS only covered specific regions.

This LSP would map the principal fine-structure FIR lines (e.g., [CII], [OI] 63 μm, [OIII] 88 μm) over a diverse range of galactic environments, including active galactic and starburst nuclei, spiral arm/interarm regions, outskirts of galaxies, HII/PDR complexes, and low-metallicity regions. Such a comprehensive view of the ISM would allow one to:

- Understand the physical processes in the ISM giving rise to these key lines, as well as the heating/cooling budgets.
- Characterize the structure and interplay between the multiple phases of the ISM, by combining line emission from the neutral/dense (e.g., [CII] and [OI] 63 μm), ionized (e.g., Hα, [NII], [OIII]), molecular (e.g., CO, [CI]), and atomic (HI) gas phases.
- Understand how different environments, ranging from regions with moderate star formation to starburst nuclei and AGN, determine the emission of the main FIR lines. These observations will serve as local templates for the rapidly growing number of $z > 1$ galaxies detected in these same lines with powerful interferometers such as ALMA and NOEMA.
- Explore the connection between the major coolants of the neutral atomic gas, the [CII] and [OI] 63 μm lines, with the heating of the gas, as traced by the FIR continuum emission and the star formation activity. This will provide key insights into the well-known problem of the "[CII]-deficit" and the question of whether [CII] can reliably be used as a star formation tracer across galaxies.
- Determine the role of metallicity in the star formation process in low metallicity environments, such as the SMC, LMC, and other nearby galaxies.

The increased mapping speed and improved point source sensitivity of the upgraded FIFI+LS will allow program completion within ~20 flights, which may be completed within two years or two SOFIA observing cycles, respectively. Thereby, FIFI+LS allows us to move from individual case studies to significant galaxy survey science; this would be prohibitively time-consuming with the current FIFI-LS (which would need ~80 flights to complete the LSP). We can compare FIFI+LS performance improvement to recent observations of FIFI-LS. Indeed, a comparable observation has already been completed with FIFI-LS for NGC6946 in [CII] by Bigiel et al.[10] This map was completed in 9.5 h total, providing a signal-to-noise ratio of 4 for a line flux of 1.3×10^{-8} W m^{-2} sr^{-1}, and an area of 56 square arc min. The same observation would have taken <2 h with FIFI+LS factoring in the sensitivity gain of at least a factor of 1.4 (to be squared when scaling observing time), the FOV increase by a factor of 1.75 and the use of more efficient observing modes that give a reduction by another factor of 1.5. The LSP contains the observations of eight more nearby galaxies. Although these galaxies are similar in size, they are about 2 to 3 times further away than NGC6946. But their angular size also roughly

scales with the distance. Therefore, we expect that within 2 h we will be able to map a whole disk at a signal depth comparable to the NGC6946 map.

The number and diversity of physical conditions in the regions that shall be mapped for this program would yield a coherent data set that will be hard to obtain through a number of smaller disconnected programs and allows addressing the following questions.

What is the physics driving the observed "FIR line deficit" in galaxies?

It is now well established that the fraction of galaxies that have lower FIR line intensities relative to the dust continuum emission increases as a function of FIR luminosity, radiation field strength, star formation efficiency, and among other parameters.[34,35,41] This is commonly known as the "FIR line deficit" problem. In the case of the [CII] line, the relative decrease of the line with respect to the FIR continuum (by up to two orders of magnitude) was first observed in (Ultra) Luminous IR Galaxies with the Infrared Space Observatory[42,43] and later on kiloparsec scale regions in normal, star-forming galaxies[10,44,45] and starbursts.[34,35]

The physical reasons behind the line deficit remain an open question, and several explanations have been proposed, including: (1) reduction of the photoelectric heating efficiency due to the charging or destruction of the small dust grains,[42,46] (2) reaching gas densities in PDR and HII regions higher than the critical density of the transitions,[47] (3) HII regions with a high ionization parameter, implying a larger fraction of the non-ionizing stellar UV is absorbed by dust, thus reducing the fraction of UV photons available to heat the neutral gas,[41,47–49] (4) a change in the ionization state of the gas due to the harsh AGN powered radiation field,[50] or (5) a combination of high ionization parameter and high FIR extinction.[32,40]

To address the FIR line deficit, we must observe varying spatial scales and probe the dominant physical conditions of the ISM. Ultimately, this requires a multi-wavelength approach where the properties of the different phases of the ISM—including metallicity, radiation field strength (FUV and ionized), AGN activity, star formation efficiency, and histories—are known. The outlined LSP would be very well suited for this purpose, with a wealth of ancillary data available including tracers of the ionized, molecular, and atomic gas phases. This will provide a unique opportunity to finally disentangle the effect of the different physical mechanisms discussed before on setting the line to FIR continuum ratio in galaxies.

How reliable is the [CII] line emission as a tracer of star formation?

The [CII] transition is the major coolant for the neutral atomic gas.[51] Therefore, it is expected that if the ISM is in thermal balance, then the [CII] line will measure the total energy input into the gas by star formation activity. Characterizing the relation between the [CII] emission and the star formation rate is particularly relevant for studies of star-forming galaxies at very high-z ($z > 4$), which are now routinely detected and spatially resolved in [CII] line emission with ALMA.[36,52,53]

In nearby dwarf and spiral galaxies, the observed relation between [CII] and SFR surface density is almost linear, with a scatter of 0.3 dex.[8,10,54] When including the more energetic and obscured environments found in (Ultra) Luminous IR Galaxies, both the slope and the scatter in the [CII]-SFR relation increase. This is a direct consequence of the "[CII]-deficit" discussed above since for (Ultra) Luminous IR Galaxies the bulk of the star formation activity is traced by the FIR emission. Due to the inclusion of galaxies from the optical IFU surveys CALIFA and MANGA, the LSP is designed to probe a parameter space that is currently unexplored: galaxies and regions within galaxies with SFR surface densities in the ~0.01 to 1 $M_\odot$ year^{-1} kpc^{-2} range. This is right in between the parameter space covered by Herschel PACS observations of kiloparsec scale regions in nearby galaxies (e.g., from KINGFISH) and (Ultra) Luminous IR Galaxies (e.g., GOALS and SHINING).

This would allow studying the nature and reliability of the [CII]-SFR relationship in the context of full optical spectroscopic information, including the exploration of dependences with metallicity, star-formation history, AGN activity, and among others.

What is the metal abundance in HII regions when measured using temperature and extinction insensitive FIR line diagnostics?

Understanding the life-cycle of metals as galaxies evolve is crucial to constrain models of chemical enrichment and explain the tightness of the mass-metallicity relation observed in

galaxies up to $z \sim 3$.[55,56] One important limitation in this type of study is the large uncertainty ($\sim$1 dex) associated with gas phase metallicity measurements due to the strong dependence on electron temperature of the optical line diagnostics.[57] One new and direct alternative to measure gas phase metal abundances is based on the FIR [OIII] lines at 52 and 88 μm. The advantage is that these lines arise from low-lying states, which are temperature-insensitive and nearly unaffected by dust extinction, and can be observed at very high-z with ALMA.[37,58]

Combining the [OIII] optical (5007 Å) and FIR (88 μm) transitions, Croxall et al.[44] successfully applied this method to measure gas phase metallicities in 7 HII regions in the nearby galaxy NGC 628. They find that the derived abundances lie right in between the two commonly used abundance scales that differ with respect to each other by a factor of $\sim$4—the empirical model[59] and the photoionization model.[60] A part of the LSP would target the [OIII] 88-μm line in a large sample of HII regions in nearby galaxies that have existing deep and spatially resolved IFU optical data. This would enable the development of a new empirical method based on the FIR [OIII] lines to measure metal abundances that are temperature insensitive and extinction free and that can be applied to very high-z galaxies.

What is the thermal pressure in the Cold Neutral Medium (CNM)? And how is it connected to the star formation process?

Dynamic and thermal processes regulate the structure of the multi-phase ISM and ultimately establish how galaxies evolve through star formation.[61] In this context, measuring the thermal pressure in the diffuse, neutral gas is of great interest to constrain models of the structure of the ISM [e.g., warm neutral medium (WNM)/CNM balance[51]] and the self-regulation of star formation on kiloparsec scales.[62,63] In the Galactic plane, the thermal pressure of the diffuse, neutral gas is found to be in the $P_{\rm th} \sim 4500$ to 6800 K cm^{-3} range based on studies of absorption features of neutral carbon and CO toward nearby stars.[64,65] Unfortunately, these methods are not available to measure $P_{\rm th}$ in nearby galaxies.

Currently, the one alternative we have to measure $P_{\rm th}$ in extragalactic sources was first proposed by Kulkarni and Heiles.[66] The method relies on the [CII] cooling rate per hydrogen nucleus ($\Lambda_{\rm [CII]}$), which in regions where the [CII] line excitation is dominated by collisions with hydrogen atoms yields the thermal pressure of the neutral, diffuse gas. Herrera-Camus et al.[67] applied this method to atomic-dominated regions in nearby galaxies and finds a median thermal pressure of $P_{\rm th}/k \sim 3600$ K cm^3, consistent with Galactic measurements. Moreover, they find that the thermal pressure is about 25% the dynamical equilibrium pressure and that this fraction is constant as a function of star formation surface density, as expected from models of self-regulated star-formation on kiloparsec scales.[62] Thanks to the significant increase in the sensitivity and mapping speed of FIFI+LS, the LSP would be designed to greatly improve the number statistics and accuracy of $P_{\rm th}$ measurements by mapping large regions in the outskirts of galaxies where the gas is atomic-dominated. These measurements will provide key constraints on the multi-phase neutral ISM structure (e.g., CNM/WNM balance), dynamical equilibrium (e.g., $P_{\rm tot}/P_{\rm th}$), and connection between the CNM atomic gas and star-formation activity.

What is the fraction of molecular gas that is not traced by CO line emission on different physical scales and galactic environments?

Analytic and numerical models suggest that the "CO-faint" H_2 resides in the translucent part of clouds, where $A_V \leq 2$ mag.[68,69] At this extinction, H_2—which is strongly self-shielding—remains molecular but most carbon still exists as C+.[15,70,71] This leads to a deficit of CO, but renders these regions visible to SOFIA in [CII] 158 μm.

This "CO-faint" phase is expected to be important even at solar metallicities and to dominate the H_2 budget at low metallicities. Studies of the SMC (1/5 solar metallicity) find that the CO-faint phase encompass 70% to 90% of all the H_2.[72–74] Given that it dominates the H_2 mass at low metallicities, our embryonic understanding of the amount of "CO-faint" H_2 and its effects on star formation is one of the largest gaps in our picture of galaxy evolution. FIFI+LS observations of the SMC in regions with deep ALMA observations of the CO line would make a significant contribution to the limited number of CO-faint H_2 studies in low-metallicity environments.

5 Conclusion

The SOFIA observatory provides an environment in which instruments can be upgraded to make use of the latest technological developments. We have presented an FIFI-LS upgrade with KIDs arrays that will take advantage of this environment to significantly improve the instrument's efficiency and increase the size of the SOFIA observable universe. The upgrade will provide 3.5 to 12 times faster observing while reducing upgrade cost by utilizing the already flying FIFI-LS instrument as its solid basis. The increased observing speed and sensitivity will allow transitioning from single/small sample observations to large sample survey programs, probing a large range of physical conditions in the ISM and star forming regions extragalactic and within the Galaxy.

Acknowledgments

SOFIA, the "Stratospheric Observatory for Infrared Astronomy," is a joint project of the Deutsches Zentrum für Luft-und Raumfahrt e.V. (DLR; German Aerospace Centre, Grant No. 50OK0901) and the National Aeronautics and Space Administration (NASA). It is funded on behalf of DLR by the Federal Ministry of Economics and Technology based on legislation by the German Parliament, the state of Baden-Württemberg, and the Universität Stuttgart. Scientific operation for Germany is coordinated by the German SOFIA-Institute (DSI) of the Universität Stuttgart, in the USA by the Universities Space Research Association (USRA). The commissioning of FIFI-LS was supported by the Bundesministerium für Wirtschaft und Technologie (Federal Ministry of Economics and Technology of the Federal Republic of Germany) through the DLR Space Administration (Grant No. 50OK1201). Frank Bigiel would like to acknowledge the funding from the European Research Council (ERC) under the European Union's Horizon 2020 Research and Innovation Program (Grant Agreement No. 726384/Empire). This work was also published in the proceedings of the SPIE Astronomical Telescopes + Instrumentation Digital Forum 2020 as SPIE Paper No. 11453-101. We would like to thank the anonymous referees for many helpful comments on an earlier draft of this manuscript.

References

1. C. Fischer et al., "FIFI-LS: the Field-Imaging Far-Infrared Line Spectrometer on SOFIA," *J. Astron. Instrum.* **7**(04), 1840003 (2018).
2. E. E. Becklin, E. T. Young, and M. L. Savage, "Stratospheric Observatory for Infrared Astronomy (SOFIA)," *Proc. SPIE* **9973**, 99730I (2016).
3. L. W. Looney et al., "Realizing integral field spectroscopy in the far-infrared," *Astrophys. J.* **597**(1), 628–643 (2003).
4. D. Rosenthal et al., "16 × 25 Ge:Ga detector arrays for FIFI LS," *Proc. SPIE* **4014**, 156–163 (2000).
5. A. Poglitsch, C. Waelkens, and N. Geis, "The Photodetector Array Camera & Spectrometer (PACS) for the Herschel Space Observatory," *Proc. SPIE* **4850**, 662–673 (2003).
6. SOFIA Science Center, "Observer's handbook for cycle 9," v.9.1.0, 2020, https://www.sofia.usra.edu/science/proposing-and-observing/observers-handbook-cycle-9.
7. J. L. Pineda et al., "A SOFIA survey of [C II] in the Galaxy M51. I. [C II] as a tracer of star formation," *Astrophys. J.* **869**, L3O (2018).
8. R. Herrera-Camus et al., "[C II] 158 μm emission as a star formation tracer," *Astrophys. J.* **800**(1), 1–22 (2015).
9. K. Kohno et al., "Diffuse and gravitationally stable molecular gas in the post-starburst galaxy NGC 5195," *Publ. Astron. Soc. Jpn.* **54**(4), 541–553 (2002).
10. F. Bigiel et al., "SOFIA/FIFI-LS full-disk [CII] mapping and CO-dark molecular gas across the nearby spiral galaxy NGC6946," *Astrophys. J.* **903**(1), 30 (2020).
11. P. N. Appleton et al., "Jet-related excitation of the [CII] emission in the active galaxy NGC4258 with SOFIA," *Astrophys. J.* **869**(1), 61 (2018).
12. I. Smirnova-Pinchukova et al., "The close AGN reference survey (CARS): discovery of a global [CII] 158 μm line excess in AGN HE 1353-1917," *Astron. Astrophys.* **626**, L3 (2019).

13. C. Iserlohe et al., "FIFI-LS observations of the circumnuclear ring: probing the high-density phase of the PDR," *Astrophys. J.* **885**(2), 169 (2019).
14. T. L. Herter et al., "FORCAST: a mid-infrared camera for SOFIA," *J. Astron. Instrum.* **7**(04), 1840005 (2018).
15. M. J. Kaufman et al., "Far-infrared and submillimeter emission from galactic and extragalactic photodissociation regions," *Astrophys. J.* **527**(2), 795 (1999).
16. S. D. Lord, "A new software tool for computing Earth's atmospheric transmission of near- and far-infrared radiation," NASA Technical Memorandum 103957 (1992).
17. C. Fischer et al., "Probing the atmospheric precipitable water vapor with SOFIA. Part I: Measurements of the Water vapor overburden with FIFI-LS," submitted to *Publ. Astron. Soc. Pac.* (2021).
18. J. Vieira et al., "The terahertz intensity mapper (TIM): an imaging spectrometer for galaxy evolution studies at high-redshift," in *30th Int. Symp. Space THz Technol.* (2019).
19. S. Hailey-Dunsheath et al., "Development of aluminum LEKIDs for balloon-borne far-IR spectroscopy," *J. Low Temp. Phys.* **193**(5–6), 968–975 (2018).
20. R. Nie et al., "Optimization of a quasi-mesh absorber for the terahertz intensity mapper," *IEEE Trans. Terahertz Sci. Technol.* **10**(6), 704–712 (2020).
21. J. Perido et al., "Extending KIDs to the mid-IR for future space and suborbital observatories," *J. Low Temp. Phys.* **199**, 696–703 (2020).
22. J. Glenn et al., "The galaxy evolution probe: a concept for a mid and far-infrared space observatory," *Proc. SPIE* **10698**, 106980L (2018).
23. S. Hailey-Dunsheath et al., "Kinetic inductance detectors for the Origins Space Telescope," *J. Astron. Telesc. Instrum. Syst.* **7**(1), 011015 (2021).
24. J. Gao et al., "Experimental evidence for surface distribution of two-level system in superconducting lithographed microwave resonators," *Appl. Phys. Lett.* **92**, 152505 (2008).
25. S. Gordon et al., "An open source, FPGA-based LeKID readout for BLAST-TNG: pre-flight results," *J. Astron. Instrum.* **5**(04), 1641003 (2016).
26. G. W. Wilson et al., "The TolTEC project: a millimeter wavelength imaging 490 polarimeter (Conference Presentation)," *Proc. SPIE* **10708**, 107080I (2018).
27. C. Risacher et al., "The upGREAT dual frequency heterodyne arrays for SOFIA," *J. Astron. Instrum.* **7**(04), 1840014 (2018).
28. J. Tuttle et al., "The HAWC and SAFIRE adiabatic demagnetization refrigerators," *Cryogenics* **41**(11), 781–787 (2001).
29. D. A. Harper et al., "HAWC+, the far-infrared camera and polarimeter for SOFIA," *J. Astron. Instrum.* **7**(04), 1840008 (2018).
30. C. D. Dowell, Personal Communication (2018).
31. TransMIT Center for Adaptive Cryotechnology and Sensors, https://cryo.transmit.de/en/products/lambda-line-pulse-tubes-two-stage-4-k-pulse-tube-cold-heads-gm-type (accessed April 2020).
32. J. Fischer et al., "A far-infrared spectral sequence of galaxies: trends and models," *Astrophys. J.* **795**(2), 117 (2014).
33. D. Cormier et al., "The Herschel Dwarf galaxy survey. I: Properties of the low-metallicity ISM from PACS spectroscopy," *Astron. Astrophys.* **578**, A53 (2015).
34. T. Díaz-Santos et al., "A Herschel/PACS far-infrared line emission survey of local luminous infrared galaxies," *Astrophys. J.* **846**(1), 1–22 (2017).
35. R. Herrera-Camus et al., "SHINING, a survey of far-infrared lines in nearby galaxies. I: Survey description, observational trends, and line diagnositcs," *Astrophys. J.* **861**(2), 1–25 (2018).
36. P. L. Capak et al., "Galaxies at redshifts 5 to 6 with systematically low dust content and high [C II] emission," *Nature* **522**, 455–458 (2015).
37. T. Hashimoto et al., "'Big three dragons': a $z = 7.15$ Lyman break galaxy detected in [OIII] 88 μm, [CII] 158 μm, and dust continuum with ALMA," *Publ. Astron. Soc. Jpn.* **71**(4), 71 (2019).
38. S. C. Madden et al., "An overview of the Dwarf galaxy survey," *Publ. Astron. Soc. Pac.* **125**(928) (2013).

39. T. Díaz-Santos et al., "The spatial extent of (U)LIRGS in the mid-infrared. II. Feature emission," *Astrophys. J.* **741**(1), 1–11 (2011).
40. E. González-Alfonso et al., "High-lying OH absorption, [C II] deficits, and extreme LFIR/MH2 ratios in galaxies," *Astrophys. J.* **800**(1), 69 (2015).
41. J. Graciá-Carpio et al., "Far-infrared line deficits in galaxies with extreme L {FIR}/M {H {2}} ratios," *Astrophys. J.* **728**(1), L7 (2011).
42. S. Malhotra et al., "Infrared space observatory measurements of [C II] line variations in galaxies," *Astrophys. J.* **491**(1), L27–L30 (1997).
43. M. Luhman et al., "Infrared space observatory measurements of a [C II] 158 micron line deficit in ultraluminous infrared galaxies," *Astrophys. J.* **504**(1), L11–L15 (2003).
44. K. V. Croxall et al., "Toward a removal of temperature dependencies from abundance determinations: NGC 628," *Astrophys. J.* **777**(2), 96 (2013).
45. J. D. T. Smith et al., "The spatially resolved [CII] cooling line deficit in galaxies," *Astrophys. J.* **834**(1), 5–5 (2016).
46. K. V. Croxall et al., "Resolving the far-IR line deficit: photoelectric heating and far-IR line cooling in NGC 1097 and NGC 4559," *Astrophys. J.* **747**(1), 81 (2012).
47. R. Herrera-Camus et al., "SHINING, a survey of far infrared lines in nearby galaxies. II: Line-deficit models, AGN impact, [CII]-SFR scaling relations, and mass-metallicity relation in (U)LIRGS," *Astrophys. J.* **861**(2), 94 (2018).
48. M. L. Luhman et al., "The [C II] 158 micron line deficit in ultraluminous infrared galaxies revisited," *Astrophys. J.* **594**(2), 758–775 (2003).
49. N. Abel et al., "Dust-bounded ultralumionous galaxies: model predictions for infrared spectroscopic surveys," *Astrophys. J.* **701**(2), 1147–1160 (2009).
50. W. D. Langer and J. L. Pineda, "[C II] emission from galactic nuclei in the presence of X-rays," *Astron. Astrophys.* **580**, A5 (2015).
51. M. G. Wolfire et al., "Neutral atomic phases of the interstellar medium in the galaxy," *Astrophys. J.* **587**(1), 278–311 (2003).
52. R. Maiolino et al., "The assembly of 'normal' galaxies at $z \sim 7$ probed by ALMA," *Mon. Not. R. Astron. Soc.* **452**(1), 54–68 (2015).
53. R. Smit et al., "Rotation in [C II]-emitting gas in two galaxies at a redshift of 6.8," *Nature* **553**, 178–181 (2018).
54. I. De Looze et al., "The applicability of far-infrared finestructure lines as star formation rate tracers over wide ranges of metallicities and galaxy types," *Astron. Astrophys.* **568**, A62 (2014).
55. C. A. Tremonti et al., "The origin of the mass-metallicity relation: insights from 53,000 star-forming galaxies in the Sloan digital sky survey," *Astrophys. J.* **613**(2), 898–913 (2004).
56. H. J. Zahid, L. J. Kewley, and F. Bresolin, "The mass-metallicity and luminosity-metallicity relations from DEEP2 at $z \sim 0.8$," *Astrophys. J.* **730**(2), 137 (2011).
57. L. J. Kewley and S. L. Ellison, "Metallicity calibrations and the mass-metallicity relation for star-forming galaxies," *Astrophys. J.* **681**(2), 1183–1204 (2008).
58. S. Carniani et al., "Kiloparsec-scale gaseous clumps and star formation at $z = 5$-7," *Mon. Not. R. Astron. Soc.* **478**(1), 1170–1184 (2018).
59. L. S. Pilyugin and T. X. Thuan, "Oxygen abundance determination in H II regions: the strong line intensities-abundance calibration revisited," *Astrophys. J.* **631**(1), 231–243 (2005).
60. H. A. Kobulnicky and L. J. Kewley, "Metallicities of $0.3 < z < 1.0$ galaxies in the GOODS-north field," *Astrophys. J.* **617**(1), 240–261 (2004).
61. L. Blitz and E. Rosolowsky, "The role of pressure in GMC formation. II: The H2-pressure relation," *Astrophys. J.* **650**(2), 933–944 (2006).
62. E. C. Ostriker, C. F. McKee, and A. K. Leroy, "Regulation of star formation rates in multiphase galactic disks: a thermal/dynamical equilibrium model," *Astrophys. J.* **721**(2), 975–994 (2010).
63. J.-G. Kim et al., "Modeling UV radiation feedback from massive stars. I: Implementation of adaptive ray-tracing method and tests," *Astrophys. J.* **851**(2), 93 (2017).
64. E. B. Jenkins and T. M. Tripp, "The distribution of thermal pressures in the diffuse, cold neutral medium of our galaxy. I: An expanded survey of interstellar C I finestructure excitations," *Astrophys. J.* **734**(1), 65 (2011).

65. P. F. Goldsmith et al., "Herschel galactic plane survey of [NII] fine structure emission," *Astrophys. J.* **814**(2), 133 (2015).
66. S. R. Kulkarni and C. Heiles, "The atomic component," in *Interstellar Processes*, D. J. Hollenbach and H. A. Thronson Jr., Eds., Vol. **134**, 87–122, Springer, Dordrecht (1987).
67. R. Herrera-Camus et al., "Thermal pressure in the cold neutral medium of nearby galaxies," *Astrophys. J.* **835**(2), 201 (2017).
68. M. G. Wolfire, D. Hollenbach, and C. F. McKee, "The dark molecular gas," *Astrophys. J.* **716**(2), 1191–1207 (2010).
69. S. C. O. Glover et al., "Modelling CO formation in the turbulent interstellar medium," *Mon. Not. R. Astron. Soc.* **404**(1), 2–29 (2009).
70. A. G. G. M. Tielens and D. Hollenbach, "Photodissociation regions. I. Basic model. II: A model for the Orion photodissociation region," *Astrophys. J.* **291**, 722–754 (1985).
71. M. G. Wolfire, D. Hollenbach, and A. G. G. M. Tielens, "The correlation of C II 158 micron and CO ($J = 1 - 0$) line emission," *Astrophys. J.* **344**, 770–778 (1989).
72. F. P. Israel, "H_2 and its relation to CO in the LMC and other magellanic irregulargalaxies," *Astron. Astrophys.* **328**, 471–482 (1997).
73. A. K. Leroy et al., "The CO-to-H_2 conversion factor from infrared dust emission across the local group," *Astrophys. J.* **737**(1), 12 (2011).
74. K. E. Jameson et al., "First results from the Herschel and ALMA spectroscopic surveys of the SMC: the relationship between [C II]-bright Gas and CO-bright gas at low metallicity," *Astrophys. J.* **853**(2), 111 (2018).

Biographies of the authors are not available.